

## Article

# Enhanced Osteogenic Activity and Antibacterial Properties of Graphene Oxide-Poly(Lactic Acid) Films for the Repair of Cranial Defects in Rats

Kai Liu <sup>1,†</sup>, Wen Lai <sup>2,†</sup>, Jianyong Wu <sup>1,\*</sup> and Yongjian Lu <sup>1,\*</sup>

<sup>1</sup> Department of Stomatology, Xinhua Hospital Affiliated to Shanghai Jiaotong University School of Medicine, Kongjiang Road 1665, Shanghai 200092, China; liukai20232023@163.com

<sup>2</sup> Shanghai Jing-An Dental Clinic, Pingxingguan Road 15, Shanghai 200070, China; laiwen2019@126.com

\* Correspondence: wujianyong@xinhumed.com.cn (J.W.); luyongjian@xinhumed.com.cn (Y.L.)

† These authors contributed equally to this work.

**Abstract:** The failure of bone defect repair caused by bacterial infection is a significant clinical challenge. However, the currently utilized bone graft materials lack antibacterial properties, necessitating the development of bone repair materials with both osteoinductive and antibacterial capabilities. Graphene oxide (GO) has garnered considerable attention due to its distinctive physical, chemical, and biological characteristics. In this study, we prepared a graphene oxide-poly(lactic acid) (GO-PLA) film with exceptional biological properties. In vitro investigations demonstrated that the GO-PLA film substantially enhanced the adhesion and proliferation capacity of rat bone marrow mesenchymal stem cells (rBMSCs). Furthermore, we observed augmented alkaline phosphatase activity as well as increased expression levels of osteogenic genes in rBMSCs cultured on the GO-PLA film. Additionally, we evaluated the antibacterial activity of our samples using gram-positive *Streptococcus mutans* (Sm) and gram-negative *Actinobacillus actinomycetemcomitans* (Aa). Our findings revealed that GO doping significantly inhibited bacterial growth. Moreover, implantation experiments conducted on rat skull defects demonstrated excellent guided bone regeneration performance exhibited by the GO-PLA film. Overall, our results indicate that the GO-PLA film possesses outstanding osteogenic and antibacterial properties, making it a promising biomaterial for bone tissue regeneration.

**Keywords:** antibacterial activity; osteogenic; graphene oxide; poly(lactic acid)



**Citation:** Liu, K.; Lai, W.; Wu, J.; Lu, Y. Enhanced Osteogenic Activity and Antibacterial Properties of Graphene Oxide-Poly(Lactic Acid) Films for the Repair of Cranial Defects in Rats.

*Coatings* **2024**, *14*, 223. <https://doi.org/10.3390/coatings14020223>

Academic Editor: Eugenio Velasco-Ortega

Received: 25 January 2024

Revised: 8 February 2024

Accepted: 10 February 2024

Published: 12 February 2024

Corrected: 6 December 2024



**Copyright:** © 2024 by the authors. Licensee MDPI, Basel, Switzerland. This article is an open access article distributed under the terms and conditions of the Creative Commons Attribution (CC BY) license (<https://creativecommons.org/licenses/by/4.0/>).

## 1. Introduction

In clinical work, the repair of bone defects caused by bacterial infection remains a significant challenge [1]. Currently, autologous bone grafting is considered the gold standard for repairing bone defects resulting from congenital malformations, tumor resection, or severe trauma. However, its application is limited due to extensive trauma, insufficient donor sites, and the risk of infection [2,3]. Therefore, there is an urgent need to develop an alternative approach that combines bone repair characteristics with anti-infection functions for effective bone tissue regeneration and inhibition of pathogenic microorganisms. Tissue engineering [4,5], an emerging discipline integrating cell biology and material science principles to construct tissues or organs in vitro or in vivo settings, has gained considerable attention. The three-dimensional structure formed by biomaterial scaffolds provides an optimal environment for cellular nutrition uptake as well as growth and metabolism. Consequently, researchers on bone scaffolds possessing both anti-infection properties and bone repair characteristics have witnessed remarkable progress in recent years [6–8].

Graphene oxide (GO) is an oxide of graphene, which is a single atomic layer with an atomic thickness that can be extended to tens of microns in cross-sectional size. Its high hydrophilic group content provides excellent dispersibility and stability [9,10]. GO exhibits significant potential in biomedical applications including multimodal bioimaging [11],

biosensors [12], and drug delivery [13]. In recent years, the exceptional biocompatibility and biodegradability of GO have garnered increasing attention [14,15]. It has been reported that GO effectively induces osteoblastic differentiation in bone marrow mesenchymal stem cells [16]. Wang et al. [17] demonstrated that surface modification of titanium implants with GO not only promotes osteogenic differentiation of BMSCs but also effectively inhibits osteoclasts. Shao et al. [18] found that the addition of GO into PLGA/tussah silk scaffolds significantly enhances the osteogenic differentiation capacity of mesenchymal stem cells (MSCs). Liu et al. [19] developed a biocompatible GO–collagen composite aerogel and observed improved mechanical properties as well as enhanced osteogenic differentiation ability in rBMSCs. Due to their multilineage differentiation potential into diverse cell types, such as osteoblasts, muscle cells, hepatocytes, chondrocytes, and others, MSCs exhibit significant promise for groundbreaking therapies in bone tissue engineering. Hence, rBMSCs were employed as seed cells for inducing osteogenic differentiation.

The misuse of conventional antibacterial drugs has resulted in the gradual emergence of bacterial drug resistance, rendering these drugs ineffective in killing bacteria. Therefore, it is crucial to identify an antibacterial agent that exhibits potent antimicrobial activity, non-resistance properties, and minimal adverse effects. GO, a two-dimensional sheet comprising oxygen groups, exhibits antibacterial activity through both nano-knife effects and reactive oxygen species [20]. Consequently, GO not only demonstrates excellent osteogenic performance but also displays effective antibacterial capabilities [21–23]. Researchers have demonstrated that GO possesses significant antibacterial efficacy against both gram-negative and gram-positive bacteria [24,25]. He et al. [21] discovered that GO exerts a strong inhibitory effect on oral pathogenic microorganisms such as *Streptococcus mutans*, *Porphyromonas gingivalis*, and *Fusobacterium nucleatum*. Qiu et al. [26] successfully deposited GO onto titanium sheets using cathodic electrophoresis and observed its efficient inhibition of bacterial activity. Unfortunately, although high concentrations of GO exhibit potent bactericidal abilities, they also induce certain levels of cytotoxicity [27]. While reducing the concentration of GO can partially alleviate cytotoxicity concerns, it may also compromise its bacteriostatic efficacy. Henceforth, we must strive to strike a delicate balance between biological safety and antimicrobial efficacy so as to achieve simultaneous osteogenic differentiation and bacteriostatic ability.

Poly(lactic acid) (PLA) is a widely utilized polymer biomaterial that can be derived through fermentation of renewable resources such as corn, starch, and potato. Its exceptional biocompatibility and degradability have led to its approval by the Food and Drug Administration (FDA) as one of the few biodegradable medical materials [28]. PLA finds extensive applications in the pharmaceutical field, including sustained-release packaging [29], surgical sutures [30] and so on. Over the past decades, PLA has been extensively employed in bone tissue regeneration research due to its remarkable biological properties [31,32]. Zhou et al. [33] demonstrated the successful design and fabrication of a 3D-printed scaffold material based on PLA, which effectively enhanced osteogenic ability in human fetal osteoblast cells (hFOB). Liu et al. [34] developed an electrospun silver nanoparticle-loaded PLA film with long-term antibacterial properties and potential for bone regeneration purposes. Han et al. [35] prepared an electrodeposited strontium-containing nanofiber film using PLA, which was found to significantly induce osteogenic differentiation of rBMSCs.

In this study, GO-PLA composite films were prepared and their antibacterial ability and osteogenic differentiation of bone marrow mesenchymal stem cells were investigated. As shown in Figure 1, pure PLA films and 0.25, 0.5, 1.0 wt% GO-PLA films were prepared by a solution casting method. *In vitro*, rBMSCs were inoculated and cultured on the scaffold to evaluate their biocompatibility and osteogenic ability. Meanwhile, two bacteria were selected to detect the antibacterial ability of GO-PLA films. Finally, bone tissue regeneration performance of GO-PLA films was studied by constructing a rat skull defect model. In summary, this study provides a theoretical basis for the application of GO in bone tissue engineering.

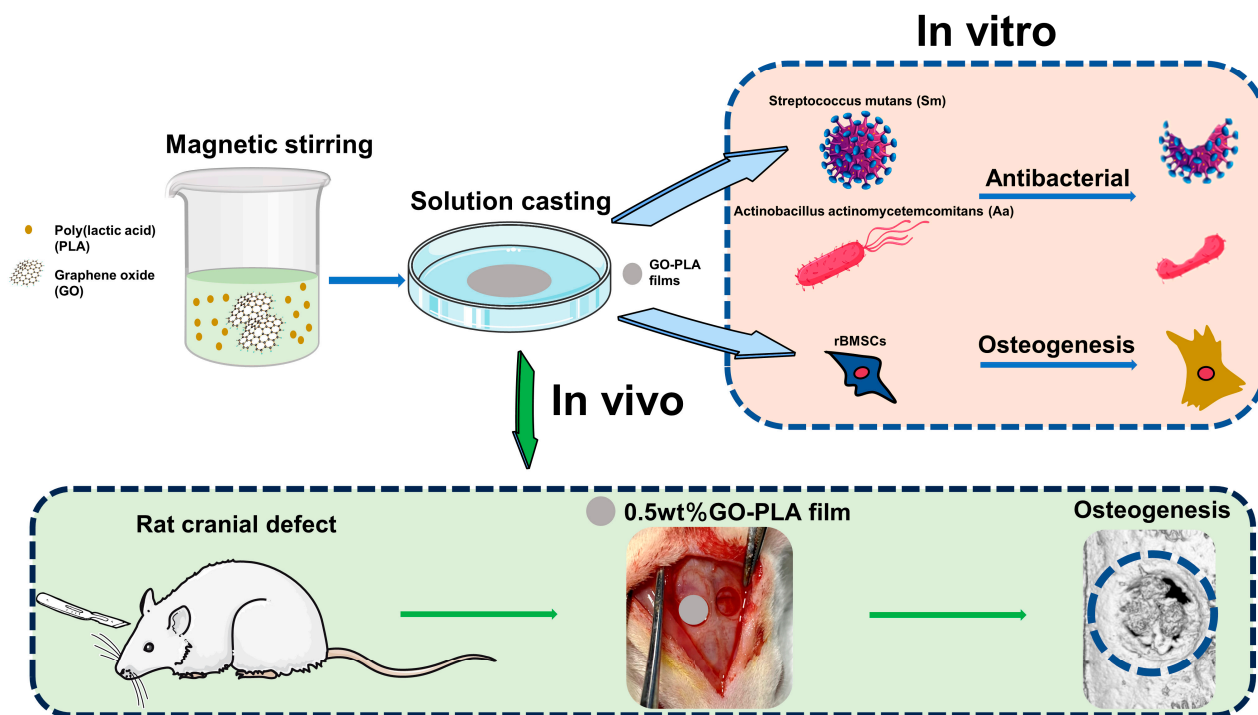


**Figure 1.** Brief schematic diagram of the preparation of the GO-PLA films, osteogenesis, and antibiosis.

## 2. Materials and Methods

### 2.1. Materials

PLA (molecular weight: 470,000) was purchased from Daigang Bio-technology Co., Ltd. (Jinan, China). GO powder was purchased from XFNANO Materials Technology Co., Ltd. (Nanjing, China). (thickness: 0.8–1.2 nm, diameter: 0.5–5  $\mu\text{m}$ ). Dichloromethane was obtained from Aladdin Industrial Co., Ltd. (Shanghai, China). Triton X-100 and trypsin were purchased from Weiao Biotechnology Co., Ltd. (Shanghai, China). Fetal bovine serum (FBS) was purchased from Gibco (Grand Island, NE, USA).  $\alpha$ -MEM, penicillin-streptomycin, phosphate-buffered saline (PBS) were purchased from HyClone (Logan, UT, USA).

### 2.2. Preparation and Characterization of the GO-PLA Films

In this experiment, GO-PLA composite films were prepared via a solution casting method. Initially, a specific amount of GO powder was added to 20 mL of dichloromethane and subjected to sonication for 3 h to achieve uniform dispersion. Subsequently, 1 g of PLA was introduced into the dispersion and vigorously stirred on a magnetic stirrer until well-mixed. The resulting mixture was then poured into preformed molds and allowed to stand undisturbed for 24 h, yielding films with varying weight percentages (0, 0.25, 0.5, and 1.0 wt%) of GO content, respectively. To eliminate any residual dichloromethane, the films underwent multiple rinses with deionized water. The functional groups of the films were observed using the Fourier transform infrared (FTIR) spectra (Thermo, Waltham, MA, USA) with a wavelength range from 2500 to 500  $\text{cm}^{-1}$ . Raman spectra with a 532 nm laser excitation was carried out using a D8 Advance (Bruker, Karlsruhe, Germany), and X-ray diffraction analysis of the films was performed at room temperature by an X-ray diffractometer (RM5, Edinburgh, UK).

### 2.3. Cell Isolation and Culture

All animal procedures in the research were approved by the Ethics Committee of Xinhua Hospital Affiliated to Shanghai Jiao Tong University School of Medicine. Rat bone marrow-derived stem cells (rBMSCs) were isolated from 4-week-old Sprague–Dawley (SD) rats as was described [36]. In a sterile environment, the femurs and tibias of SD

rats' hind limbs were isolated, and the cartilages located at both ends of the bones were excised. Subsequently, the bone marrow was flushed into a 10 cm culture dish with  $\alpha$ -MEM medium containing 10% fetal bovine serum and 1% penicillin-streptomycin solution. The dish was then placed in a cell culture incubator at 37 °C with 5% CO<sub>2</sub> and 95% humidity for cultivation. After three days, the medium was replaced, followed by subsequent replacements every two days. When the cell density reached 70%–80%, trypsin was used for subculture of the cells. P3–P4 passage cells were selected for all subsequent experiments.

#### 2.4. Cell Adhesion Activity Assay

The BMSCs were seeded onto the surface of the PLA and GO-PLA films at a density of  $1 \times 10^4$  cells/mL. After incubation for 1, 4, and 24 h, the cells were washed three times with PBS. Subsequently, they were fixed with 4% paraformaldehyde for 30 min and washed again with PBS three times. Then, permeabilization was performed using 0.1% Triton X-100 followed by blocking with a solution containing 1% bovine serum albumin for one hour. After washing three times with PBS, the cells were incubated in the dark with fluorescein-isothiocyanate-labeled phalloidin (Sigma, St. Louis, MO, USA) for 30 min and stained with DAPI for an additional five minutes. Finally, images were captured under an inverted fluorescence microscope.

#### 2.5. Cell Proliferation Measurement

The cell viability of rBMSCs cultured on PLA and GO-PLA films with varying concentrations was evaluated using the CCK-8 assay kit (Beyotime, Shanghai, China). Initially, rBMSCs were seeded onto the film surface at a density of  $1 \times 10^4$  cells/mL. After 1, 4, and 7 days of culture, the supernatant was discarded from the culture plates and subsequently subjected to three rounds of PBS washing for a duration of 5 min per wash. Subsequently, each well in a plate was supplemented with 200  $\mu$ L of cell culture medium containing a 10% CCK-8 solution and incubated in a light-shielded constant temperature incubator for 3 h. Then, 150  $\mu$ L of supernatant was transferred to a separate 96-well plate, and its optical density (OD) value was measured at a wavelength of 450 nm using a microplate reader.

#### 2.6. ALP Staining and ALP Activity Assay

rBMSCs were seeded onto the PLA and GO-PLA films in a six-well plate at a density of  $2 \times 10^4$  cells/well for alkaline phosphatase (ALP) staining. After incubation for 7 and 14 days, the cells were fixed with 4% paraformaldehyde for 30 min and washed three times with PBS. A BCIP/NBT staining solution (Beyotime, China) was prepared according to the manufacturer's instructions and added to each well, covering the cells in the six-well plate. After avoiding light exposure for 30 min, photographs were captured.

For ALP activity assay, rBMSCs were seeded onto the PLA and GO-PLA films at a density of  $1 \times 10^4$  cells/well. Following incubation for 7 and 14 days, cell lysis was performed using Triton X-100 (0.1%). The total protein content was extracted using BCA protein assay kit (Jiancheng, Nanjing, China), following the manufacturer's instructions at an absorbance wavelength of 562 nm. ALP activity was measured by detecting optical density (OD) values at a wavelength of 520 nm using an ALP activity detection kit (Beyotime, China). As we previously described [37], normalization of ALP activity was performed against total protein content.

#### 2.7. Real-Time Quantitative Polymerase Chain Reaction Analysis

##### 2.7.1. RNA Extraction

rBMSCs ( $5 \times 10^4$  cells/well) were plated and cultured for 3 and 10 days before RT-PCR analysis of the relative mRNA expression of osteogenic genes. Total RNA was isolated with 800  $\mu$ L TRIZOL reagent (TAKARA, Dalian, China) in accordance with the manufacturer's protocol. All the RNA samples used in this research had OD<sub>260/280</sub> ratio above 1.8.

### 2.7.2. RT-PCR Analysis

Total RNA extraction from rBMSCs was performed using TRIZOL reagent, and 1 µg RNA was reverse transcribed into complementary DNA in accordance with the recommendations of the manufacturer (TAKARA, Ichikawa, Japan). Expression was quantified by using Universal SYBR Green Master (Roche, Basel, Switzerland). The gene assays were performed in triplicate for each experimental group, with the expression level of GAPDH serving as an internal control. Each reaction was performed in triplicate. The primers selected are listed in Table 1.

**Table 1.** Primer sequences used for real-time PCR.

Gene	Forward Primer (5'-3')	Reverse Primer (5'-3')
Vinculin	TGGACGGCAAAGCCATTCC	GCTGGTGGCATATCTCTCTTCAG
BMP2	AACGAGAAAAGCGTCAAGCC	CCAGTCATTCCACCCCACA
OCN	CATCTATGGCACCACCGTTTA	CTGTGCCGTCCATACTTTCG
OPN	TGGATGAACCAAGCGTGGA	TCCGCTGACTGTTCGATAGCA
GAPDH	GGCAAGTTCAACGGCACAGT	GCCAGTAGACTCCACGACAT

### 2.8. Antibacterial Assay In Vitro

*Actinobacillus actinomycetemcomitans* (Aa, G<sup>-</sup>) and *Streptococcus mutans* (Sm, G<sup>+</sup>) were selected as research subjects to assess their antibacterial activities against different samples. The bacteria were cultured in brain-heart infusion broth (BHI) at a concentration of 3.7% (Sigma), under anaerobic conditions with an atmosphere consisting of 80% N<sub>2</sub>, 10% H<sub>2</sub>, and 10% CO<sub>2</sub> at a temperature of 37 °C. Following a 24-h incubation period, the bacteria were dislodged from the various films. Untreated BHI medium was considered the control group. Subsequently, the resuspended bacterial suspension was serially diluted using BHI and transferred onto agar plates for further cultivation over another period of 24 h. Finally, the antibacterial efficacy was determined by calculating colony-forming units (CFU).

### 2.9. In Vivo Osseointegration Assessment

#### 2.9.1. Animals and Surgical Procedure

The animal surgeries in this experiment were conducted in accordance with the requirements of the Institutional Animal Care and Use Committee at Shanghai Jiaotong University and received approval from the ethics committee. The rats were housed under controlled conditions at 21 °C, 50% humidity, and a light/dark cycle of 12 h. All animal experiments were carried out at the Experimental Animal Center of Xinhua Hospital, strictly adhering to welfare and ethical guidelines for experimental animals.

Twelve male SD rats, with an average weight of 200 g, were selected to establish a cranial defect model following the standard procedure [38]. The rats were randomly divided into three groups: the blank control group, where no treatment was applied to the cranial defect; the PLA group, where a PLA film was placed at the site of the cranial defect; and the 0.5 wt% GO-PLA group, where a 0.5 wt% GO-PLA film was placed at the site of the cranial defect. Initially, inhalation anesthesia (2% isoflurane) was administered followed by an intraperitoneal injection of 1% pentobarbital sodium at a dose of 50 mg/kg in rats. The rat's head was disinfected with iodine solution before making a midline incision along with skin and periosteum separation to expose the skull bone. A circular full-thickness bone defect with a diameter of 4 mm was symmetrically created on both sides along the sagittal suture using a circular burr with a diameter of 4 mm. After completing bone defect preparation, either PLA or 0.5 wt% GO-PLA film was implanted into the defect area while leaving some defects without any material as blank controls. Skin and periosteum tissues were sutured layer by layer using absorbable sutures for alignment purposes. Eight weeks after surgery, three groups of rats were sacrificed, and their cranial specimens were fixed in 4% paraformaldehyde (PFA) for subsequent studies.

### 2.9.2. Micro-CT Assay

Trim the separated rat skull samples to appropriate sizes and perform micro-CT scanning using a voxel size of 7  $\mu\text{m}$  with the VENUS micro-CT system (Pingsheng Scientific, Suzhou, China). Subsequently, employ three-dimensional reconstruction software to obtain reconstructed new bone formation at the defect site along with X-ray image data. Calculate bone volume (BV) and bone volume/total volume ratio (BV/TV) within the same range as the defect.

### 2.9.3. Histological Observation

After Micro-CT scanning, all samples were decalcified using ethylenediaminetetraacetic acid (EDTA) solution (Beyotime, China) for a duration of 4 weeks. Subsequently, the decalcified samples underwent dehydration with ethanol and were embedded in paraffin. Histological analysis was conducted on tissue sections measuring 5  $\mu\text{m}$  in thickness from the central region of the cranial bone defect. In accordance with the manufacturer's instructions, these tissue sections were stained using hematoxylin-eosin (HE) and Masson's trichrome stain. Observation and photography procedures were performed under an optical microscope (Nikon, Tokyo, Japan).

### 2.10. Statistical Analysis

The data were presented as mean  $\pm$  standard deviation (SD). Group differences were analyzed using one-way analysis of variance (ANOVA). A  $p$ -value less than 0.05 was considered statistically significant.

## 3. Results

### 3.1. Characterization of the Graphene Oxide-Incorporated-PLA Films

The GO-PLA films depicted in Figure 2A exhibit distinct characteristics. While the pure PLA films displayed a milky white color, the GO-PLA films exhibited a gradual darkening of color with increasing GO content from 0.25 to 1.0 wt%. Initially, both the pure PLA and GO-PLA films were subjected to FTIR analysis for characterization purposes (Figure 2B). The presence of specific peaks confirmed the existence of various functional groups within these films: an asymmetric bending of carbonyl (C=O) at 1750  $\text{cm}^{-1}$ , an asymmetric stretching of -C-CH<sub>3</sub> at 1451  $\text{cm}^{-1}$ . The peak positions of 1380 and 1360  $\text{cm}^{-1}$  represent symmetric and asymmetric bending of -C-H. 1181 and 1083  $\text{cm}^{-1}$  represent symmetric and asymmetric bending of C-O-C, while -OH group representation at 1042  $\text{cm}^{-1}$ , stretching of -CH<sub>3</sub> at 956  $\text{cm}^{-1}$ , and stretching of -C-C at 870  $\text{cm}^{-1}$  [39]. These observed peaks validate the presence of PLA in all film samples. The successful incorporation of GO into the PLA nanofibers was confirmed by the Raman spectra, as depicted in Figure 2C. In the GO-containing films, distinct peaks corresponding to the D and G bands were observed at 1345 and 1600  $\text{cm}^{-1}$ , respectively. Additionally, a peak at 1766  $\text{cm}^{-1}$  could be attributed to the C=O stretching of carboxyl groups in PLA molecules, while another peak at 1450  $\text{cm}^{-1}$  represented the -CH<sub>3</sub> asymmetric deformation of the repeating unit. The X-ray diffraction (XRD) patterns of pure PLA and GO-PLA films are presented in Figure 2D. In the XRD pattern of GO-PLA films, a distinct and intense peak is observed at  $2\theta \approx 11^\circ$ , indicating the presence of oxidized graphite functional groups. This peak corresponds to an interlayer spacing of 0.79 nm, which is characteristic of layered GO structures. Overall, the results from FTIR, Raman spectroscopy, and XRD analysis unequivocally demonstrate the successful integration of GO into PLA films.

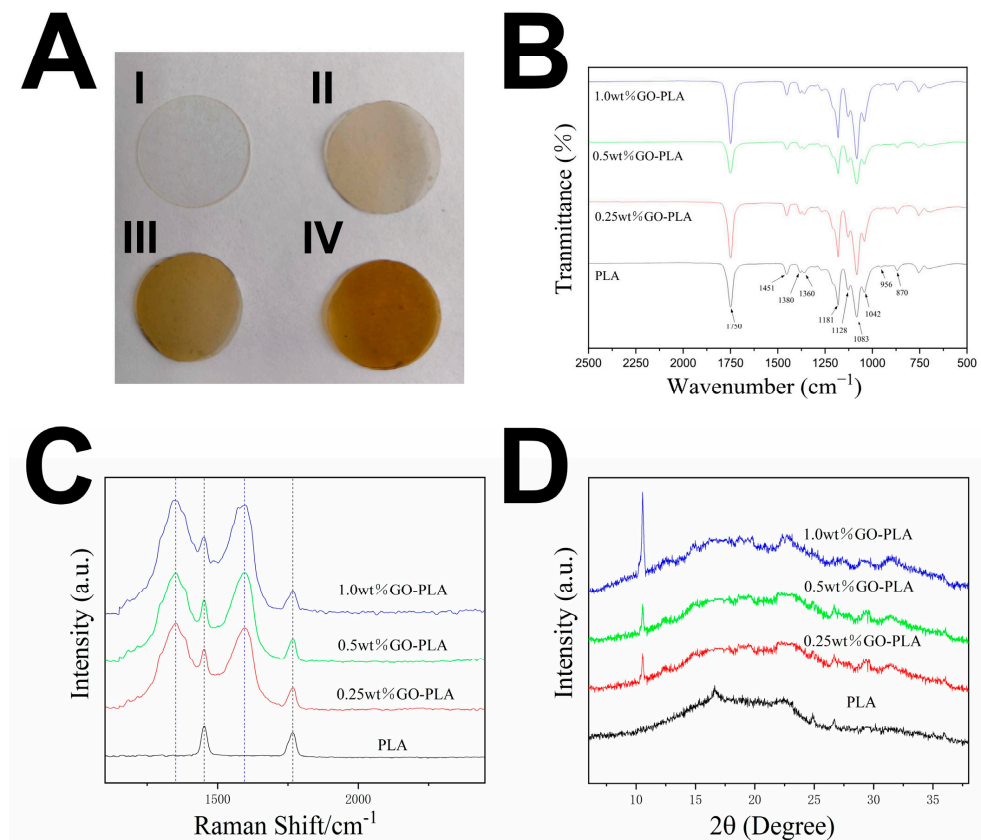


**Figure 2.** Characterization of the PLA and 0.25/0.5/1.0 wt% GO-PLA films. (A) Images of PLA (I), 0.25 wt% GO-PLA (II), 0.5 wt% GO-PLA (III), and 1.0 wt% GO-PLA (IV), respectively. (B) FTIR, (C) Raman, and (D) XRD analyses of the PLA and GO-PLA films.

### 3.2. Effect of Graphene Oxide Incorporation on the Adhesion and Proliferation of rBMSCs on PLA Films

After culturing rBMSCs on pure PLA and GO-PLA films for 1, 4, and 24 h, the morphology of rBMSCs was examined using immunofluorescence staining to investigate the impact of GO incorporation on cell adhesion. As depicted in Figure 3A, cells exhibited a spindle-shaped morphology with fewer pseudopodia on the surface of the pure PLA film, indicating weak affinity between rBMSCs and the pure PLA film. Conversely, on the surfaces of 0.25, 0.5 and 1.0 wt% GO-PLA films, cells displayed well-spread morphologies with significantly extended filamentous pseudopodia, suggesting that GO could enhance rBMSCs' adhesion ability. Additionally, RT-PCR analysis was conducted to assess vinculin gene expression as a focal adhesion protein level in rBMSCs. The results demonstrated higher vinculin gene expression in rBMSCs cultured on GO-PLA films compared to those cultured on the pure PLA film (Figure 3B), with the highest expression observed in the 0.5 wt% GO-PLA group. To evaluate how GO incorporation affected rBMSCs proliferation activity, cell viability was assessed using CCK-8 after culture periods of 1, 4, and 7 days. As illustrated in Figure 3C, the proliferation activity of cells cultured on GO-PLA films was higher than that observed in the pure PLA group; notably, the highest activity was observed in the presence of a concentration of 0.5 wt% GO within PLA.

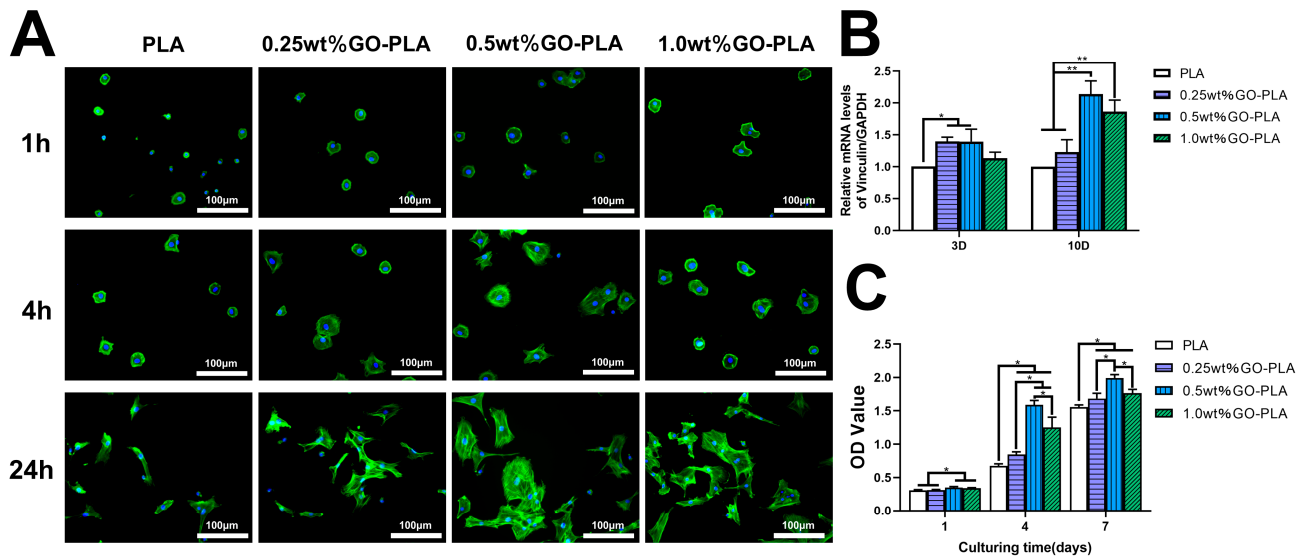


**Figure 3.** Cell adhesion and proliferation assay. (A) Fluorescence images of rBMSCs cultured on the PLA and GO-PLA films surface after 1, 4 and 24 h of incubation. (B) Vinculin gene expression of rBMSCs cultured for 3 and 10 days. (C) Cell proliferation of rBMSCs cultured for 1, 4 and 7 days. (\*)  $p < 0.05$ , (\*\*)  $p < 0.01$ . (scale bar = 100  $\mu\text{m}$ ).

### 3.3. Effect of Graphene Oxide Incorporation on the ALP Activity and Osteogenic-Related Genes Expression of rBMSCs on PLA Films

The expression of ALP, a marker indicating pre-osteogenic differentiation, was evaluated by conducting ALP staining and measuring its activity at two time points (3 and 10 days) on both pure PLA film and GO-PLA films with varying concentrations. The results demonstrated that (Figure 4A) the depth of ALP staining in the 0.25, 0.5, and 1.0 wt% GO-PLA films were significantly higher than that in the pure PLA film group, particularly at 0.5 wt% GO-PLA film. Similar trends were observed at days 14. Additionally, quantitative ALP activity detection (Figure 4B) revealed higher ALP activity in all GO-PLA films compared to pure PLA film, with the highest levels observed in the 0.5 wt% GO-PLA group. Furthermore, real-time fluorescence quantitative PCR was conducted at days 3 and 10 to assess expression levels of osteogenic marker genes (BMP2, OCN, OPN) in rBMSCs cultured on GO-PLA films. After three days of culture, it became evident that the expression levels of BMP2, OCN, and OPN in the 0.5 wt% GO-PLA group exhibited significantly higher values compared to the other three groups (Figure 4C–E). No statistically significant difference was observed between the expression levels of BMP2 and OPN in rBMSCs among the 0.25 and 1.0 wt% GO-PLA groups and the pure PLA group. However, for OCN expression level in rBMSCs, both the 0.25 and 0.5 wt% GO-PLA groups demonstrated higher values than the remaining two groups; furthermore, with an increase in GO concentration, a decrease in relative expression level was observed specifically within the 1.0 wt% GO-PLA group. Upon reaching a culture period of ten days, there was an upregulation of BMP2 and OPN expression levels in rBMSCs on all three types of GO-PLA films when compared to the control group; notably, this effect was most pronounced within the 0.5 wt% GO-PLA group. As for OCN expression level, both the 0.5 and 1.0 wt% GO-PLA groups displayed higher values than their counterparts; however, it is worth mentioning that the higher values were recorded in the 0.5 wt% GO-PLA film.

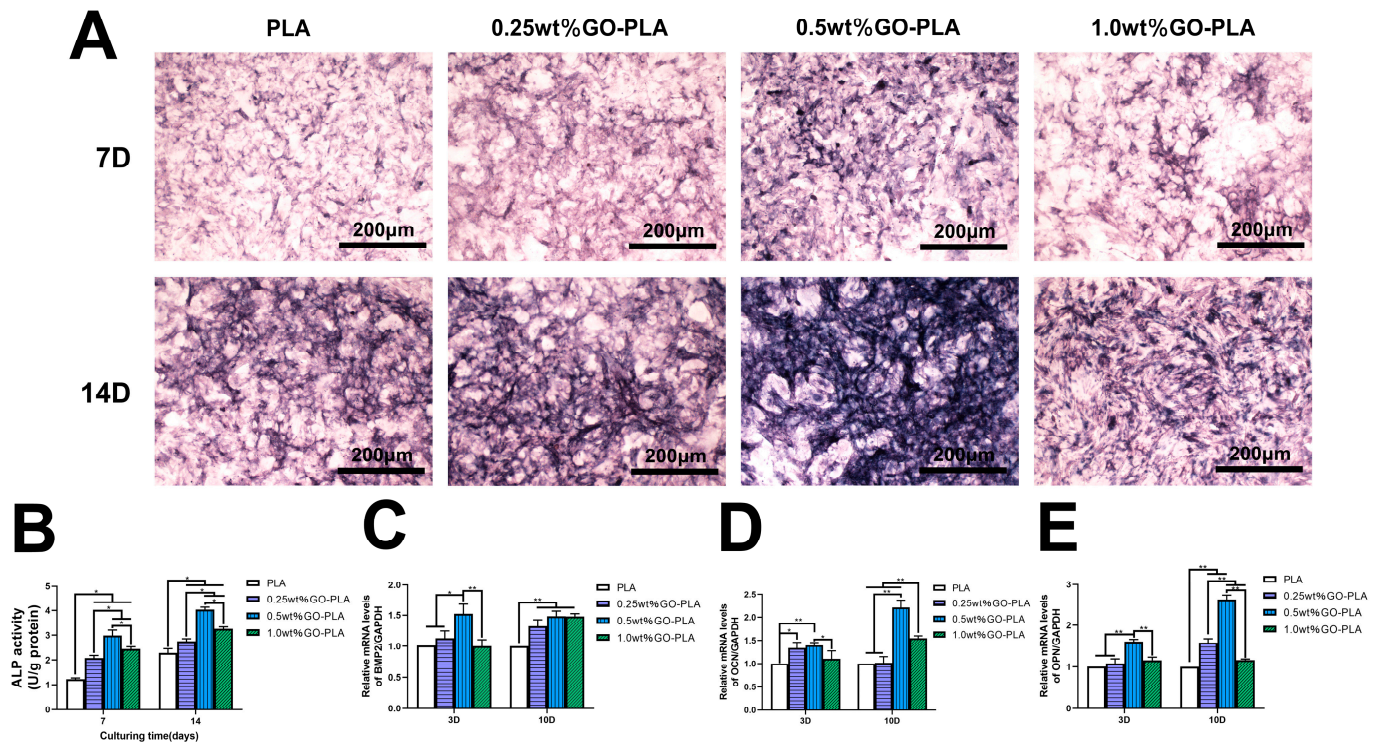


**Figure 4.** Osteogenic differentiation of rBMSCs cultured on the PLA and GO-PLA films. (A) ALP staining and (B) ALP activity of rBMSCs incubated on different films for 7 and 14 days. (C–E) Osteogenic-related genes expression in rBMSCs cultured for 3 and 10 days: (C) BMP2, (D) OCN, (E) OPN. (\*)  $p < 0.05$ , (\*\*)  $p < 0.01$ . (scale bar = 200  $\mu\text{m}$ ).

### 3.4. Effect of Graphene Oxide Incorporation on the Antibacterial Activity on PLA Films

The in vitro antibacterial performance of 0.5 wt% GO-PLA film was tested using two representative oral bacteria, namely gram-positive bacteria Sm and gram-negative bacteria Aa. As depicted in Figure 5A, the control group and PLA group exhibited a large number of colonies that covered almost the entire bacterial culture plate; however, the number of colonies in the 0.5 wt% GO-PLA group was significantly lower than that in the other two groups. Colony counting analysis revealed that the inhibition rate of the 0.5 wt% GO-PLA film on Aa exceeded 80% (Figure 5B). Effective inhibition on Sm by the 0.5 wt% GO-PLA film was also observed, as shown in Figure 5C,D. Subsequently, scanning electron microscopy (SEM) was employed to record bacterial morphology (Figure 5E). In both control and PLA groups, Aa and Sm maintained their normal size, shape, and intact cell membranes; flagella were even visible on Aa indicating active motility. Conversely, when cultured on the 0.5 wt% GO-PLA film, bacterial cell walls and membranes lost their integrity with leakage of intracellular contents; no flagella were observed either. Similarly, exposure to the 0.5 wt% GO-PLA film resulted in a collapsed and fragmented structure for Sm suggesting direct damage caused by this material.

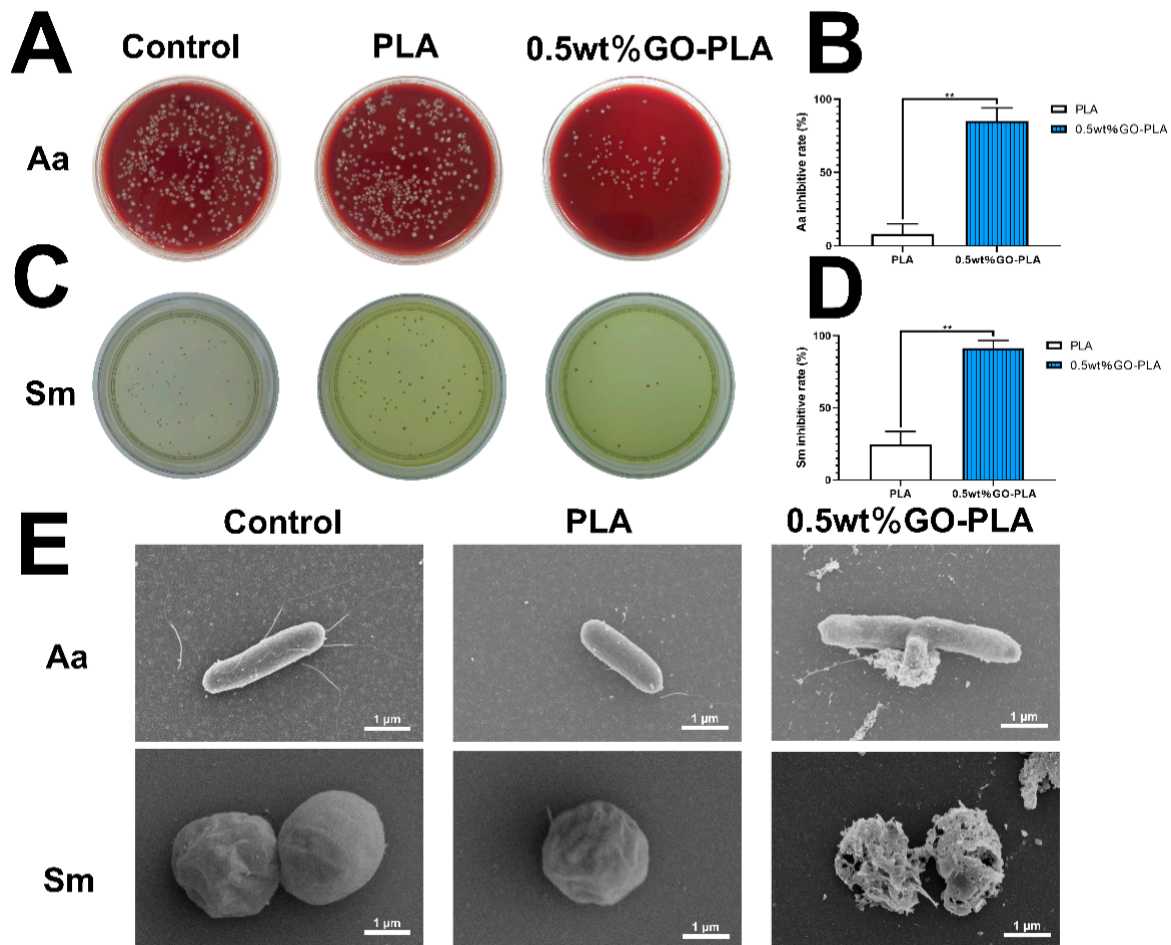


**Figure 5.** Antibacterial activity of PLA and 0.5 wt% GO-PLA films. Photographs of recultivated (A) Aa and (C) Sm colonies cultured on the PLA and 0.5 wt% GO-PLA films for 24 h. (B,D) Analysis of reduction percentages of bacteria colonies. (E) SEM images of Aa and Sm cells. (\*\*)  $p < 0.01$ . (scale bar = 1  $\mu\text{m}$ ).

### 3.5. Guiding the Bone Tissue Regeneration of Graphene Oxide-Incorporated PLA Films In Vivo

The role of film-guided bone regeneration was investigated in a rat skull defect model, with the untreated group serving as the control. After 8 weeks of implanting the films into the rat skull defect, micro-CT scanning was performed to observe the regenerated bone. As depicted in Figure 6A, three-dimensional reconstruction revealed minimal new bone formation in the blank control group compared to its initial size (4 mm diameter indicated by blue circle), while both experimental groups exhibited greater new bone growth than the control group. Notably, the 0.5 wt% GO-PLA film demonstrated nearly complete closure of the bone defect area, indicating significantly enhanced new bone regeneration compared to the pure PLA film alone. Figure 6B,C illustrate newly formed bone volume (BV) and ratio of BV to total volume (BV/TV), respectively. The results demonstrate superior outcomes for both pure PLA and 0.5 wt% GO-PLA films over the blank control group. Moreover, at a concentration of 0.5 wt%, GO induced more new bone generation than pure PLA alone. Histological analysis through HE and Masson staining on decalcified specimens further supported these findings (Figure 7). In all samples, new bone formation was considerably lower in the blank control group compared to both experimental groups, with most areas being covered by soft tissue only. Partial coverage with newly formed bone was observed in the pure PLA group; however, it was most pronounced in the 0.5 wt% GO-PLA group which exhibited extensive new bone growth relative to other groups examined herein.

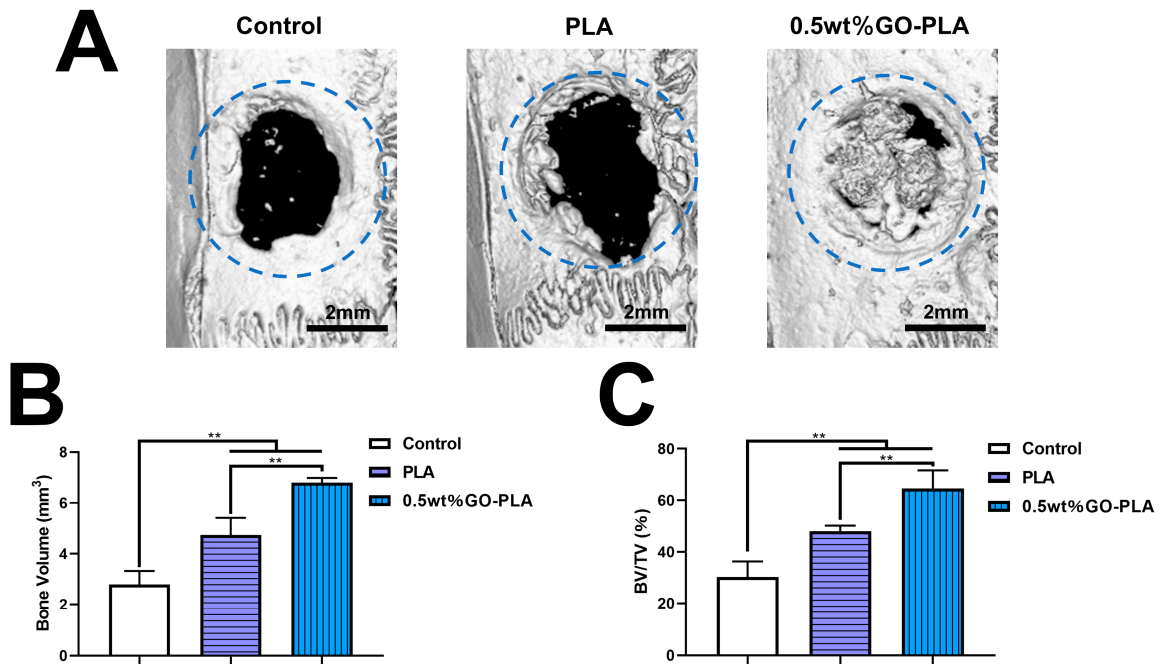


**Figure 6.** Micro-CT evaluation of rat cranial bone defects in vivo. (A) Representative CT reconstruction images of skull defects 8 weeks post-implantation (4 mm diameter indicated by blue circle). (B) Bone volume and (C) bone volume to tissue volume (BV/TV) analysis.  $n = 3$ . (\*\*\*)  $p < 0.01$ . (scale bar = 2 mm).

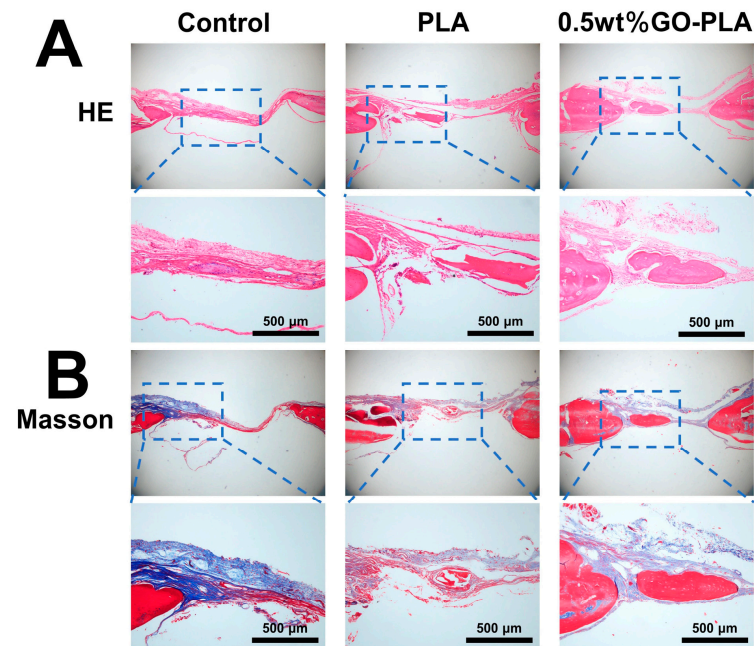


**Figure 7.** Histological analysis of bone regeneration. (A) H&E and (B) Masson staining images of rat calvarial defect regions 8 weeks post-implantation. (scale bar = 500 μm).

#### 4. Discussion

Bone defect repair poses a significant challenge in the field of orthopedics due to the high risk of treatment failure caused by bacterial infection [40,41]. However, conventional bone graft materials lack antibacterial properties, thereby impeding effective bone regeneration [42]. In routine clinical practice, combining antibiotics with bone graft materials is the most common approach for treating infectious bone defects [43,44]. Nevertheless,

antibiotics fail to effectively combat complex infections caused by drug-resistant bacteria and partially inhibit the osteogenic induction of bone graft materials [45–47], leading to compromised anti-infection and bone defect repair outcomes. To address this issue, there is an urgent need for the development of novel transplant materials with dual functionality that can fulfill both antibacterial and osteogenic requirements. Therefore, we have designed and synthesized a GO-loaded PLA film aiming to enhance the antibacterial activity and potential for bone tissue regeneration in bone graft materials.

In recent years, graphene and graphene oxide(GO)-based materials have emerged as a prominent area of focus in medical research [4,48]. GO exhibits distinctive physical and chemical characteristics encompassing remarkable mechanical robustness, abundant oxygen-functional groups, and a high ratio of surface area. These attributes enable it to play a pivotal role in various biomedical engineering applications [48], nanomedicine advancements [49], tumor therapy strategies [50], drug release systems [51], and biological imaging techniques [52], among others. Compared to other spherical or flat nanomaterials, GO exhibits a significantly larger specific surface area along with superior strength and excellent biocompatibility. Bone marrow mesenchymal stem cells serve as crucial precursor cells for osteoblasts and play an essential role in bone regeneration and integration processes [53]. The recruitment and adhesion of BMSCs represent the initial stages of osteogenesis while also being closely associated with cell proliferation and osteogenic differentiation. Therefore, we selected rBMSCs as the seed cells for this study to investigate the osteogenic properties of GO. To accomplish this objective, three different concentrations of 0.25, 0.5 and 1.0 wt% were employed while utilizing pure PLA film as the control group.

As depicted in Figure 3A, the extended area of rBMSCs cultured on GO-PLA films with concentrations of 0.25, 0.5 and 1.0 wt% were found to be larger compared to that on pure PLA film, accompanied by a significant extension of filamentous pseudopodia, particularly evident on the 0.5 wt% GO-PLA film. Furthermore, RT-PCR quantitative analysis (Figure 3B) revealed a substantial increase in the expression level of vinculin, a cell adhesion plaque protein, in the GO-modified films. These findings indicate that GO effectively enhances the cell adhesion ability of rBMSCs, which is consistent with previous studies by Li et al. [54]. Notably, it is worth mentioning that the expression level of vinculin was lower in the 1.0 wt% GO-PLA film compared to that in the 0.5 wt% GO-PLA film. Consistent results were obtained from cell counting kit-8 (CCK-8) assay as well; when using a concentration of 1.0 wt% GO, rBMSCs exhibited lower proliferation activity than those cultured on the 0.5 wt% GO-PLA film. This suggests that high concentrations of GO moderately inhibit cell adhesion and activity. Wang et al. [55] synthesized GO using a modified Hummers method and evaluated its cytotoxicity on human skin fibroblasts. The results demonstrated that GO exhibited low cytotoxicity at a concentration of 20  $\mu\text{g}/\text{mL}$ ; however, upon increasing the concentration to 50  $\mu\text{g}/\text{mL}$ , there was a significant decrease in cell viability. Cicuéndez et al. [56] employed fluorescein-labeled GO nanosheets to investigate the cellular uptake by MC3T3-E1 pre-osteoblasts, which resulted in reduced cell proliferation and increased apoptosis. Some researchers hypothesized that the abundance of oxygen-containing functional groups on the surface of GO could generate reactive oxygen species (ROS), leading to toxic effects on cells through activation of the caspase cascade reaction [57]. Therefore, it is crucial to explore an optimal concentration of GO that promotes both cell proliferation and osteogenesis.

ALP staining and quantification of ALP activity were employed to assess the early osteogenic potential of rBMSCs on various films. ALP serves as not only a participant in the mineralization process but also an important marker for early osteogenesis [58]. Following 7 and 14 days of culture, the GO-incorporated scaffolds exhibited more intense staining compared to the control group, indicating that GO significantly enhanced ALP expression, particularly in 0.5 wt% GO-PLA films (Figure 4A). This finding was further supported by quantitative analysis of ALP activity, which demonstrated increased expression across all concentrations of GO-PLA films (Figure 4B).

Moreover, to gain deeper insights into the impact of GO on osteogenic differentiation, we also evaluated the expression levels of BMP2, OCN, and OPN as key osteogenic genes. The results revealed that GO promoted their expression; however, higher concentration (1.0 wt%) GO-PLA films displayed lower gene expression compared to those with a concentration of 0.5 wt% (Figure 4C–E). BMP2, a member of the TGF- $\beta$  superfamily, plays a pivotal role in osteogenesis and chondrogenesis by effectively inducing mesenchymal cell differentiation into osteoblasts [59]. OPN, an essential bone matrix protein widely distributed in the extracellular matrix, is closely associated with bone development and formation [60]. OCN emerges towards the end of osteoblast differentiation; it binds to  $\text{Ca}^{2+}$  ions to regulate calcium homeostasis and promote bone mineralization while also contributing to the maturation and mineralization processes of osteoblasts [61]. Numerous studies have demonstrated that GO composites possess regenerative properties for nerves [62], blood vessels [63], and particularly for bone tissues [17]. This may be attributed to abundant functional groups on GO surfaces providing a unique platform for promoting osteogenesis through various pathways such as PI3K/Akt/GSK-3 $\beta$ / $\beta$ -catenin signaling pathway, actin cytoskeleton dynamics or ERK signaling pathway [64,65].

Infection following bone graft implantation is a significant contributor to bone graft failure. Recently, GO has garnered considerable attention due to its exceptional bactericidal properties. Based on the results of in vitro cytological experiments, we selected the 0.5 wt% GO-PLA film with varying concentrations of GO ranging from 0.25 to 1.0 wt% for subsequent bacterial experiments, while the untreated group served as the control group. In this study, Aa and Sm were chosen as the research subjects, and bacterial counting was employed to evaluate their antibacterial efficacy. As depicted in Figure 5A–D, compared to both the control group and pure PLA film, the 0.5 wt% GO-PLA film effectively suppressed the proliferation of Aa and Sm bacteria. Scanning electron microscopy (SEM) was utilized to observe bacterial morphology and membrane integrity on different film surfaces (Figure 5E). The bacterial morphology in the 0.5 wt% GO-PLA group exhibited loss of integrity with broken and wrinkled films. These findings demonstrate that GO-modified samples possess excellent antibacterial effects. Guo et al. [66] prepared a coating (SPEEK-GO) by depositing GO on the surface of Poly-ether-ether-ketone (PEEK). The bactericidal efficacy of SPEEK-GO against *P. gin-givalis* was determined to be  $80.75\% \pm 2.54\%$ , while that against *S. mutans* was found to be  $66.41\% \pm 3.87\%$ . Sun et al. [67] reported a modification of the surface of titanium implants (Ti-MAO-GO) using microarc oxidation (MAO) combined with self-assembled graphene oxide (GO). The antibacterial rate of Ti-MAO-GO against *S. mutans* was determined to be  $93.25\% \pm 2.47\%$ . Currently, a consensus regarding the antibacterial mechanism of GO has not yet been reached. Several prominent mechanisms for its bactericidal activity have been proposed, encompassing oxidative stress induced by reactive oxygen species (ROS) generation [23], nano-knife effect and charge transfer phenomena [68], as well as interactions with phospholipids [69], proteins [70], and DNA/RNA molecules [71], among others.

In vivo osteogenic capacity plays a crucial role in assessing the osteogenic potential of biomaterials. In this study, we established a rat skull defect model with a 4 mm diameter to investigate the osteogenic efficacy of GO-PLA films. A blank control group without any treatment was included as the control. Consistent with our in vitro findings, implantation of 0.5 wt% GO-PLA films significantly enhanced bone tissue regeneration compared to both the blank control and pure PLA film after an 8-week period without exogenous growth factors supplementation, as demonstrated by micro-CT reconstruction results (Figure 6A). Subsequently, statistical analysis was performed on bone volume and bone volume to tissue volume ratio (BV/TV) (Figure 6B,C), revealing that the 0.5 wt% GO-PLA film exhibited superior ability for bone tissue generation compared to pure PLA film, with statistically significant differences observed. This finding was further confirmed through histological staining analysis. HE staining and Masson staining results revealed minimal new bone matrix in the blank control group after 8 weeks of scaffold implantation, while significant new bone formation was observed in the pure PLA film group. In contrast, the 0.5 wt%

GO-PLA group exhibited a thickened new bone matrix that occupied most of the defect area. These findings were consistent with micro-CT results and further substantiated the exceptional osteogenic potential of the 0.5 wt% GO-PLA film. This phenomenon may be attributed to the ability of GO to significantly enhance rBMSCs' osteogenic differentiation, as well as its capacity within the scaffold to facilitate rBMSCs and biomolecule adsorption, thereby promoting cell adhesion, proliferation, and differentiation for enhanced new bone formation. The findings of this study are consistent with those reported by other researchers. Liu et al. [19] fabricated a GO-based collagen composite aerogel and observed a significant enhancement in bone formation in a rat skull defect model upon the addition of GO. Srinivetha et al. [72] developed a nanocomposite incorporating GO and demonstrated that the scaffolds containing GO exhibited superior efficacy in promoting bone defect healing. However, there are still numerous unresolved issues pertaining to the clinical application of graphene and its derivatives that necessitate further exploration. It is imperative to elucidate the factors influencing the biosafety of graphene and its derivatives, as well as to delve into their underlying mechanisms in greater detail. Presently, our understanding regarding strategies for minimizing host immune responses to these composites and comprehending the impact of graphene and its derivatives on inflammation remains limited. Furthermore, additional research is required to investigate the potential utilization of graphene and its derivatives in clinically repairing bone defects. In summary, our study highlights the exceptional osteogenic and antibacterial properties of the GO-PLA film, which holds great promise for bone tissue regeneration applications. Therefore, the GO-PLA film represents a highly prospective material for repairing bone defects.

## 5. Conclusions

In summary, we have successfully prepared GO-modified PLA films. In vitro results showed that GO-PLA films could enhance cell adhesion compared with the pure PLA film. In addition, when the concentration of GO increased to 0.5 wt%, it could significantly enhance the proliferation of rBMSCs, but when the concentration was further increased to 1.0 wt%, the proliferation of rBMSCs decreased. At the same time, the addition of GO not only promoted the expression of ALP, but also increased the expression levels of other osteogenesis-related genes. GO-modified PLA films had good antibacterial ability, which could effectively inhibit the proliferation of gram-positive bacteria *Sm* and gram-negative bacteria *Aa*. Moreover, the results of in vivo animal model further confirmed that GO-PLA films could effectively promote the regeneration of bone tissue. In conclusion, our study has proved that GO-PLA film is a potential bone tissue biomaterial.

**Author Contributions:** Conceptualization, K.L.; methodology, W.L.; data curation, K.L.; writing—original draft preparation, K.L. and W.L.; writing—review and editing, J.W. and Y.L.; project administration, J.W.; funding acquisition, Y.L. All authors have read and agreed to the published version of the manuscript.

**Funding:** The present study was financially supported by Xinhua Hospital Affiliated to Shanghai Jiaotong University School of Medicine Rolling fund for scientific research and Development (GD202112).

**Institutional Review Board Statement:** The experimental protocol employed in this study was granted approval by the Ethics Committee of Xinhua Hospital Affiliated to Shanghai Jiao Tong University School of Medicine (approval number: XHEC-F-2022-066).

**Informed Consent Statement:** Not applicable.

**Data Availability Statement:** The data presented in this study are available on request from the corresponding author.

**Conflicts of Interest:** The authors declare no conflict of interest.

## References

1. Jia, Z.; Xiu, P.; Xiong, P.; Zhou, W.; Cheng, Y.; Wei, S.; Zheng, Y.; Xi, T.; Cai, H.; Liu, Z.; et al. Additively Manufactured Macroporous Titanium with Silver-Releasing Micro-/Nanoporous Surface for Multipurpose Infection Control and Bone Repair—A Proof of Concept. *ACS Appl. Mater. Interfaces* **2016**, *8*, 28495–28510. [[CrossRef](#)]
2. Yang, Y.; Chu, L.; Yang, S.; Zhang, H.; Qin, L.; Guillaume, O.; Eglin, D.; Richards, R.G.; Tang, T. Dual-Functional 3D-Printed Composite Scaffold for Inhibiting Bacterial Infection and Promoting Bone Regeneration in Infected Bone Defect Models. *Acta Biomater.* **2018**, *79*, 265–275. [[CrossRef](#)]
3. Majidinia, M.; Sadeghpour, A.; Yousefi, B. The Roles of Signaling Pathways in Bone Repair and Regeneration. *J. Cell. Physiol.* **2018**, *233*, 2937–2948. [[CrossRef](#)]
4. Ou, L.; Tan, X.; Qiao, S.; Wu, J.; Su, Y.; Xie, W.; Jin, N.; He, J.; Luo, R.; Lai, X.; et al. Graphene-Based Material-Mediated Immunomodulation in Tissue Engineering and Regeneration: Mechanism and Significance. *ACS Nano* **2023**, *17*, 18669–18687. [[CrossRef](#)]
5. Koushik, T.M.; Miller, C.M.; Antunes, E. Bone Tissue Engineering Scaffolds: Function of Multi-Material Hierarchically Structured Scaffolds. *Adv. Healthc. Mater.* **2023**, *12*, 2202766. [[CrossRef](#)]
6. Lu, Y.; Li, L.; Zhu, Y.; Wang, X.; Li, M.; Lin, Z.; Hu, X.; Zhang, Y.; Yin, Q.; Xia, H.; et al. Multifunctional Copper-Containing Carboxymethyl Chitosan/Alginate Scaffolds for Eradicating Clinical Bacterial Infection and Promoting Bone Formation. *ACS Appl. Mater. Interfaces* **2018**, *10*, 127–138. [[CrossRef](#)]
7. Chen, M.; Li, Y.; Hou, W.-X.; Peng, D.-Y.; Li, J.-K.; Zhang, H.-X. The Antibacterial Effect, Biocompatibility, and Osteogenesis of Vancomycin-Nanodiamond Composite Scaffold for Infected Bone Defects. *Int. J. Nanomed.* **2023**, *18*, 1365–1380. [[CrossRef](#)]
8. Yao, H.; Wang, J.; Deng, Y.; Li, Z.; Wei, J. Osteogenic and Antibacterial PLLA Membrane for Bone Tissue Engineering. *Int. J. Biol. Macromol.* **2023**, *247*, 125671. [[CrossRef](#)]
9. Loh, K.P.; Bao, Q.; Eda, G.; Chhowalla, M. Graphene Oxide as a Chemically Tunable Platform for Optical Applications. *Nat. Chem.* **2010**, *2*, 1015–1024. [[CrossRef](#)]
10. Park, S.Y.; Park, J.; Sim, S.H.; Sung, M.G.; Kim, K.S.; Hong, B.H.; Hong, S. Enhanced Differentiation of Human Neural Stem Cells into Neurons on Graphene. *Adv. Mater.* **2011**, *23*, H263–H267. [[CrossRef](#)]
11. Chawda, N.; Basu, M.; Majumdar, D.; Poddar, R.; Mahapatra, S.K.; Banerjee, I. Engineering of Gadolinium-Decorated Graphene Oxide Nanosheets for Multimodal Bioimaging and Drug Delivery. *ACS Omega* **2019**, *4*, 12470–12479. [[CrossRef](#)]
12. Tian, X.; Hu, J.; Wei, T.; Ding, W.; Miao, Q.; Ning, Z.; Fan, S.; Wu, H.; Lu, J.; Lyu, M.; et al. Fast and Sensitive Graphene oxide-DNAzyme-based Biosensor for *Vibrio Alginolyticus* Detection. *J. Fish. Dis.* **2022**, *45*, 687–697. [[CrossRef](#)]
13. Karki, N.; Tiwari, H.; Tewari, C.; Rana, A.; Pandey, N.; Basak, S.; Sahoo, N.G. Functionalized Graphene Oxide as a Vehicle for Targeted Drug Delivery and Bioimaging Applications. *J. Mater. Chem. B* **2020**, *8*, 8116–8148. [[CrossRef](#)]
14. Holt, B.D.; Wright, Z.M.; Arnold, A.M.; Sydlik, S.A. Graphene Oxide as a Scaffold for Bone Regeneration. *WIREs Nanomed. Nanobiotechnol.* **2017**, *9*, e1437. [[CrossRef](#)]
15. Yang, J.-W.; Hsieh, K.Y.; Kumar, P.V.; Cheng, S.-J.; Lin, Y.-R.; Shen, Y.-C.; Chen, G.-Y. Enhanced Osteogenic Differentiation of Stem Cells on Phase-Engineered Graphene Oxide. *ACS Appl. Mater. Interfaces* **2018**, *10*, 12497–12503. [[CrossRef](#)]
16. Li, Q.; Shen, A.; Wang, Z. Enhanced Osteogenic Differentiation of BMSCs and M2-Phenotype Polarization of Macrophages on a Titanium Surface Modified with Graphene Oxide for Potential Implant Applications. *RSC Adv.* **2020**, *10*, 16537–16550. [[CrossRef](#)]
17. Wang, H.; Lai, Y.; Xie, Z.; Lin, Y.; Cai, Y.; Xu, Z.; Chen, J. Graphene Oxide-Modified Concentric Microgrooved Titanium Surfaces for the Dual Effects of Osteogenesis and Antiosteoclastogenesis. *ACS Appl. Mater. Interfaces* **2022**, *14*, 54500–54516. [[CrossRef](#)]
18. Shao, W.; He, J.; Wang, Q.; Cui, S.; Ding, B. Biomimetic Poly(L-Lactic-Co-Glycolic Acid)/Graphene Oxide/Tussah Silk Fibroin Nanofiber Scaffolds with Multiple Orthogonal Layers Enhance Osteoblastic Differentiation of Mesenchymal Stem Cells. *ACS Biomater. Sci. Eng.* **2017**, *3*, 1370–1380. [[CrossRef](#)]
19. Liu, S.; Zhou, C.; Mou, S.; Li, J.; Zhou, M.; Zeng, Y.; Luo, C.; Sun, J.; Wang, Z.; Xu, W. Biocompatible Graphene Oxide–Collagen Composite Aerogel for Enhanced Stiffness and in Situ Bone Regeneration. *Mater. Sci. Eng. C* **2019**, *105*, 110137. [[CrossRef](#)]
20. Panda, S.; Rout, T.K.; Prusty, A.D.; Ajayan, P.M.; Nayak, S. Electron Transfer Directed Antibacterial Properties of Graphene Oxide on Metals. *Adv. Mater.* **2018**, *30*, 1702149. [[CrossRef](#)]
21. He, J.; Zhu, X.; Qi, Z.; Wang, C.; Mao, X.; Zhu, C.; He, Z.; Li, M.; Tang, Z. Killing Dental Pathogens Using Antibacterial Graphene Oxide. *ACS Appl. Mater. Interfaces* **2015**, *7*, 5605–5611. [[CrossRef](#)]
22. Zou, F.; Zhou, H.; Jeong, D.Y.; Kwon, J.; Eom, S.U.; Park, T.J.; Hong, S.W.; Lee, J. Wrinkled Surface-Mediated Antibacterial Activity of Graphene Oxide Nanosheets. *ACS Appl. Mater. Interfaces* **2017**, *9*, 1343–1351. [[CrossRef](#)]
23. Liu, S.; Zeng, T.H.; Hofmann, M.; Burcombe, E.; Wei, J.; Jiang, R.; Kong, J.; Chen, Y. Antibacterial Activity of Graphite, Graphite Oxide, Graphene Oxide, and Reduced Graphene Oxide: Membrane and Oxidative Stress. *ACS Nano* **2011**, *5*, 6971–6980. [[CrossRef](#)]
24. Pulingam, T.; Thong, K.L.; Ali, M.E.; Appaturi, J.N.; Dinshaw, I.J.; Ong, Z.Y.; Leo, B.F. Graphene Oxide Exhibits Differential Mechanistic Action towards Gram-Positive and Gram-Negative Bacteria. *Colloids Surf. B Biointerfaces* **2019**, *181*, 6–15. [[CrossRef](#)]
25. Song, C.; Yang, C.-M.; Sun, X.-F.; Xia, P.-F.; Qin, J.; Guo, B.-B.; Wang, S.-G. Influences of Graphene Oxide on Biofilm Formation of Gram-Negative and Gram-Positive Bacteria. *Environ. Sci. Pollut. Res.* **2018**, *25*, 2853–2860. [[CrossRef](#)]
26. Qiu, J.; Geng, H.; Wang, D.; Qian, S.; Zhu, H.; Qiao, Y.; Qian, W.; Liu, X. Layer-Number Dependent Antibacterial and Osteogenic Behaviors of Graphene Oxide Electrophoretic Deposited on Titanium. *ACS Appl. Mater. Interfaces* **2017**, *9*, 12253–12263. [[CrossRef](#)]

27. Zhang, Y.; Ali, S.F.; Dervishi, E.; Xu, Y.; Li, Z.; Casciano, D.; Biris, A.S. Cytotoxicity Effects of Graphene and Single-Wall Carbon Nanotubes in Neural Phaeochromocytoma-Derived PC12 Cells. *ACS Nano* **2010**, *4*, 3181–3186. [[CrossRef](#)]
28. Li, G.; Zhao, M.; Xu, F.; Yang, B.; Li, X.; Meng, X.; Teng, L.; Sun, F.; Li, Y. Synthesis and Biological Application of Polylactic Acid. *Molecules* **2020**, *25*, 5023. [[CrossRef](#)] [[PubMed](#)]
29. Haroosh, H.J.; Dong, Y.; Jasim, S.; Ramakrishna, S. Improvement of Drug Release and Compatibility between Hydrophilic Drugs and Hydrophobic Nanofibrous Composites. *Materials* **2021**, *14*, 5344. [[CrossRef](#)]
30. Deng, X.; Gould, M.; Ali, M.A. A Review of Current Advancements for Wound Healing: Biomaterial Applications and Medical Devices. *J. Biomed. Mater. Res.* **2022**, *110*, 2542–2573. [[CrossRef](#)] [[PubMed](#)]
31. Li, X.; Jin, Q.; Xu, H.; Zhang, S.; Wang, W.; Zhao, B. Effect of Polylactic Acid Membrane on Guided Bone Regeneration in Anterior Maxillary Implantation. *Med. Sci. Monit.* **2023**, *29*, e938566. [[CrossRef](#)] [[PubMed](#)]
32. Jang, H.J.; Kang, M.S.; Kim, W.-H.; Jo, H.J.; Lee, S.-H.; Hahm, E.J.; Oh, J.H.; Hong, S.W.; Kim, B.; Han, D.-W. 3D Printed Membranes of Polylactic Acid and Graphene Oxide for Guided Bone Regeneration. *Nanoscale Adv.* **2023**, *5*, 3619–3628. [[CrossRef](#)] [[PubMed](#)]
33. Zhou, X.; Zhou, G.; Junka, R.; Chang, N.; Anwar, A.; Wang, H.; Yu, X. Fabrication of Polylactic Acid (PLA)-Based Porous Scaffold through the Combination of Traditional Bio-Fabrication and 3D Printing Technology for Bone Regeneration. *Colloids Surf. B Biointerfaces* **2021**, *197*, 111420. [[CrossRef](#)] [[PubMed](#)]
34. Liu, F.; Cheng, X.; Xiao, L.; Wang, Q.; Yan, K.; Su, Z.; Wang, L.; Ma, C.; Wang, Y. Inside-Outside Ag Nanoparticles-Loaded Polylactic Acid Electrospun Fiber for Long-Term Antibacterial and Bone Regeneration. *Int. J. Biol. Macromol.* **2021**, *167*, 1338–1348. [[CrossRef](#)] [[PubMed](#)]
35. Han, X.; Zhou, X.; Qiu, K.; Feng, W.; Mo, H.; Wang, M.; Wang, J.; He, C. Strontium-Incorporated Mineralized PLLA Nanofibrous Membranes for Promoting Bone Defect Repair. *Colloids Surf. B Biointerfaces* **2019**, *179*, 363–373. [[CrossRef](#)] [[PubMed](#)]
36. Wang, Z.X.; Chen, C.; Zhou, Q.; Wang, X.S.; Zhou, G.; Liu, W.; Zhang, Z.-Y.; Cao, Y.; Zhang, W.J. The Treatment Efficacy of Bone Tissue Engineering Strategy for Repairing Segmental Bone Defects Under Osteoporotic Conditions. *Tissue Eng. Part A* **2015**, *21*, 2346–2355. [[CrossRef](#)]
37. Yu, Y.; Liu, K.; Wen, Z.; Liu, W.; Zhang, L.; Su, J. Double-Edged Effects and Mechanisms of Zn<sup>2+</sup> Microenvironments on Osteogenic Activity of BMSCs: Osteogenic Differentiation or Apoptosis. *RSC Adv.* **2020**, *10*, 14915–14927. [[CrossRef](#)]
38. Spicer, P.P.; Kretlow, J.D.; Young, S.; Jansen, J.A.; Kasper, F.K.; Mikos, A.G. Evaluation of Bone Regeneration Using the Rat Critical Size Calvarial Defect. *Nat. Protoc.* **2012**, *7*, 1918–1929. [[CrossRef](#)]
39. Dong, X.; Liang, X.; Zhou, Y.; Bao, K.; Sameen, D.E.; Ahmed, S.; Dai, J.; Qin, W.; Liu, Y. Preparation of Polylactic Acid/TiO<sub>2</sub>/GO Nano-Fibrous Films and Their Preservation Effect on Green Peppers. *Int. J. Biol. Macromol.* **2021**, *177*, 135–148. [[CrossRef](#)]
40. Chen, Z.-Y.; Gao, S.; Zhang, Y.-W.; Zhou, R.-B.; Zhou, F. Antibacterial Biomaterials in Bone Tissue Engineering. *J. Mater. Chem. B* **2021**, *9*, 2594–2612. [[CrossRef](#)]
41. Ren, G.; Li, R.; Hu, Y.; Chen, Y.; Chen, C.; Yu, B. Treatment Options for Infected Bone Defects in the Lower Extremities: Free Vascularized Fibular Graft or Ilizarov Bone Transport? *J. Orthop. Surg. Res.* **2020**, *15*, 439. [[CrossRef](#)]
42. Gristina, A.G. Biomaterial-Centered Infection: Microbial Adhesion Versus Tissue Integration. *Science* **1987**, *237*, 1588–1595. [[CrossRef](#)]
43. Hai, J.H.; Lee, C.; Kapila, Y.L.; Chaffee, B.W.; Armitage, G.C. Antibiotic Prescribing Practices in Periodontal Surgeries with and without Bone Grafting. *J. Periodontol.* **2020**, *91*, 508–515. [[CrossRef](#)]
44. Hussain, S.; Joo, J.; Kang, J.; Kim, B.; Braun, G.B.; She, Z.-G.; Kim, D.; Mann, A.P.; Mölder, T.; Teesalu, T.; et al. Antibiotic-Loaded Nanoparticles Targeted to the Site of Infection Enhance Antibacterial Efficacy. *Nat. Biomed. Eng.* **2018**, *2*, 95–103. [[CrossRef](#)]
45. Franci, G.; Falanga, A.; Galdiero, S.; Palomba, L.; Rai, M.; Morelli, G.; Galdiero, M. Silver Nanoparticles as Potential Antibacterial Agents. *Molecules* **2015**, *20*, 8856–8874. [[CrossRef](#)]
46. Wang, L.; Hu, C.; Shao, L. The Antimicrobial Activity of Nanoparticles: Present Situation and Prospects for the Future. *Int. J. Nanomed.* **2017**, *12*, 1227–1249. [[CrossRef](#)]
47. Khodabukus, A.; Guyer, T.; Moore, A.C.; Stevens, M.M.; Guldborg, R.E.; Bursac, N. Translating Musculoskeletal Bioengineering into Tissue Regeneration Therapies. *Sci. Transl. Med.* **2022**, *14*, eabn9074. [[CrossRef](#)]
48. Xiao, Y.; Pang, Y.X.; Yan, Y.; Qian, P.; Zhao, H.; Manickam, S.; Wu, T.; Pang, C.H. Synthesis and Functionalization of Graphene Materials for Biomedical Applications: Recent Advances, Challenges, and Perspectives. *Adv. Sci.* **2023**, *10*, 2205292. [[CrossRef](#)]
49. Bhatt, S.; Punetha, V.D.; Pathak, R.; Punetha, M. Graphene in Nanomedicine: A Review on Nano-Bio Factors and Antibacterial Activity. *Colloids Surf. B Biointerfaces* **2023**, *226*, 113323. [[CrossRef](#)]
50. Shi, D.; Zhuang, J.; Fan, Z.; Zhao, H.; Zhang, X.; Su, G.; Xie, L.; Ge, D.; Hou, Z. Self-Targeting Nanotherapy Based on Functionalized Graphene Oxide for Synergistic Thermochemotherapy. *J. Colloid Interface Sci.* **2021**, *603*, 70–84. [[CrossRef](#)]
51. Itoo, A.M.; Vemula, S.L.; Gupta, M.T.; Giram, M.V.; Kumar, S.A.; Ghosh, B.; Biswas, S. Multifunctional Graphene Oxide Nanoparticles for Drug Delivery in Cancer. *J. Control. Release* **2022**, *350*, 26–59. [[CrossRef](#)]
52. Lin, J.; Chen, X.; Huang, P. Graphene-Based Nanomaterials for Bioimaging. *Adv. Drug Deliv. Rev.* **2016**, *105*, 242–254. [[CrossRef](#)]
53. Petrochenko, P.E.; Zhang, Q.; Bayati, R.; Skoog, S.A.; Phillips, K.S.; Kumar, G.; Narayan, R.J.; Goering, P.L. Cytotoxic Evaluation of Nanostructured Zinc Oxide (ZnO) Thin Films and Leachates. *Toxicol. Vitro.* **2014**, *28*, 1144–1152. [[CrossRef](#)]
54. Li, Q.; Wang, Z. Involvement of FAK/P38 Signaling Pathways in Mediating the Enhanced Osteogenesis Induced by Nano-Graphene Oxide Modification on Titanium Implant Surface. *Int. J. Nanomed.* **2020**, *15*, 4659–4676. [[CrossRef](#)]

55. Wang, K.; Ruan, J.; Song, H.; Zhang, J.; Wo, Y.; Guo, S.; Cui, D. Biocompatibility of Graphene Oxide. *Nanoscale Res. Lett.* **2010**, *6*, 8. [[CrossRef](#)]
56. Cicuéndez, M.; Silva, V.S.; Hortigüela, M.J.; Matesanz, M.C.; Vila, M.; Portolés, M.T. MC3T3-E1 Pre-Osteoblast Response and Differentiation after Graphene Oxide Nanosheet Uptake. *Colloids Surf. B Biointerfaces* **2017**, *158*, 33–40. [[CrossRef](#)]
57. Zhang, W.; Wang, C.; Li, Z.; Lu, Z.; Li, Y.; Yin, J.; Zhou, Y.; Gao, X.; Fang, Y.; Nie, G.; et al. Unraveling Stress-Induced Toxicity Properties of Graphene Oxide and the Underlying Mechanism. *Adv. Mater.* **2012**, *24*, 5391–5397. [[CrossRef](#)]
58. Wang, Q.; Li, M.; Cui, T.; Wu, R.; Guo, F.; Fu, M.; Zhu, Y.; Yang, C.; Chen, B.; Sun, G. A Novel Zwitterionic Hydrogel Incorporated with Graphene Oxide for Bone Tissue Engineering: Synthesis, Characterization, and Promotion of Osteogenic Differentiation of Bone Mesenchymal Stem Cells. *Int. J. Mol. Sci.* **2023**, *24*, 2691. [[CrossRef](#)]
59. Ao, Q.; Wang, S.; He, Q.; Ten, H.; Oyama, K.; Ito, A.; He, J.; Javed, R.; Wang, A.; Matsuno, A. Fibrin Glue/Fibronectin/Heparin-Based Delivery System of BMP2 Induces Osteogenesis in MC3T3-E1 Cells and Bone Formation in Rat Calvarial Critical-Sized Defects. *ACS Appl. Mater. Interfaces* **2020**, *12*, 13400–13410. [[CrossRef](#)]
60. Bailey, S.; Karsenty, G.; Gundberg, C.; Vashishth, D. Osteocalcin and Osteopontin Influence Bone Morphology and Mechanical Properties. *Ann. N. Y. Acad. Sci.* **2017**, *1409*, 79–84. [[CrossRef](#)]
61. Marom, R.; Shur, I.; Solomon, R.; Benayahu, D. Characterization of Adhesion and Differentiation Markers of Osteogenic Marrow Stromal Cells. *J. Cell. Physiol.* **2005**, *202*, 41–48. [[CrossRef](#)]
62. Hui, Y.; Yan, Z.; Yang, H.; Xu, X.; Yuan, W.-E.; Qian, Y. Graphene Family Nanomaterials for Stem Cell Neurogenic Differentiation and Peripheral Nerve Regeneration. *ACS Appl. Bio Mater.* **2022**, *5*, 4741–4759. [[CrossRef](#)]
63. Bayaraa, O.; Dashnyam, K.; Singh, R.K.; Mandakhbayar, N.; Lee, J.H.; Park, J.-T.; Lee, J.-H.; Kim, H.-W. Nanoceria-GO-Intercalated Multicellular Spheroids Revascularize and Salvage Critical Ischemic Limbs through Anti-Apoptotic and pro-Angiogenic Functions. *Biomaterials* **2023**, *292*, 121914. [[CrossRef](#)]
64. Wu, X.; Zheng, S.; Ye, Y.; Wu, Y.; Lin, K.; Su, J. Enhanced Osteogenic Differentiation and Bone Regeneration of Poly(Lactic-Co-Glycolic Acid) by Graphene via Activation of PI3K/Akt/GSK-3 $\beta$ / $\beta$ -Catenin Signal Circuit. *Biomater. Sci.* **2018**, *6*, 1147–1158. [[CrossRef](#)]
65. Luo, Y.; Shen, H.; Fang, Y.; Cao, Y.; Huang, J.; Zhang, M.; Dai, J.; Shi, X.; Zhang, Z. Enhanced Proliferation and Osteogenic Differentiation of Mesenchymal Stem Cells on Graphene Oxide-Incorporated Electrospun Poly(Lactic-Co-Glycolic Acid) Nanofibrous Mats. *ACS Appl. Mater. Interfaces* **2015**, *7*, 6331–6339. [[CrossRef](#)]
66. Guo, C.; Lu, R.; Wang, X.; Chen, S. Antibacterial activity, bio-compatibility and osteogenic differentiation of graphene oxide coating on 3D-network poly-ether-ether-ketone for orthopaedic implants. *J. Mater. Sci. Mater. Med.* **2021**, *32*, 135. [[CrossRef](#)]
67. Sun, N.; Yin, S.; Lu, Y.; Zhang, W.; Jiang, X. Graphene oxide-coated porous titanium for pulp sealing: An antibacterial and dentino-inductive restorative material. *J. Mater. Chem. B* **2020**, *8*, 5606–5619. [[CrossRef](#)]
68. Zou, X.; Zhang, L.; Wang, Z.; Luo, Y. Mechanisms of the Antimicrobial Activities of Graphene Materials. *J. Am. Chem. Soc.* **2016**, *138*, 2064–2077. [[CrossRef](#)]
69. Tu, Y.; Lv, M.; Xiu, P.; Huynh, T.; Zhang, M.; Castelli, M.; Liu, Z.; Huang, Q.; Fan, C.; Fang, H.; et al. Destructive extraction of phospholipids from Escherichia coli membranes by graphene nanosheets. *Nat. Nanotech.* **2013**, *8*, 594–601. [[CrossRef](#)]
70. Alava, T.; Mann, J.A.; Théodore, C.; Benitez, J.J.; Dichtel, W.R.; Parpia, J.M.; Craighead, H.G. Control of the Graphene-Protein Interface Is Required to Preserve Adsorbed Protein Function. *Anal. Chem.* **2013**, *85*, 2754–2759. [[CrossRef](#)]
71. Mohammed, H.; Kumar, A.; Bekyarova, E.; Al-Hadeethi, Y.; Zhang, X.; Chen, M.; Ansari, M.S.; Cochis, A.; Rimondini, L. Antimicrobial Mechanisms and Effectiveness of Graphene and Graphene-Functionalized Biomaterials. A Scope Review. *Front. Bioeng. Biotechnol.* **2020**, *8*, 465. [[CrossRef](#)] [[PubMed](#)]
72. Pathmanapan, S.; Periyathambi, P.; Anandasadagopan, S.K. Fibrin hydrogel incorporated with graphene oxide functionalized nanocomposite scaffolds for bone repair—In vitro and in vivo study. *Nanomед. Nanotechnol. Biol. Med.* **2020**, *29*, 102251. [[CrossRef](#)] [[PubMed](#)]

**Disclaimer/Publisher’s Note:** The statements, opinions and data contained in all publications are solely those of the individual author(s) and contributor(s) and not of MDPI and/or the editor(s). MDPI and/or the editor(s) disclaim responsibility for any injury to people or property resulting from any ideas, methods, instructions or products referred to in the content.